Journal of High Energy Physics, Gravitation and Cosmology, 2026, 12(1), 17-33
https://www.scirp.org/journal/jhepgc
ISSN Online: 2380-4335
ISSN Print: 2380-4327

Excitation Spectra of Alkali Atoms under Spatially Confined Core Potentials

Olokunboyo A. Olaiya

Department of Physics and Astronomy, University of New Hampshire, Durham, NH, USA
Email: olokunboyoabiolade@gmail.com

How to cite this paper: Olaiya, O.A. (2026) Excitation Spectra of Alkali Atoms under Spatially Confined Core Potentials. *Journal of High Energy Physics, Gravitation and Cosmology*, **12**, 17-33.
https://doi.org/10.4236/jhepgc.2026.121002

Received: August 12, 2025
Accepted: December 6, 2025
Published: December 9, 2025

Abstract

This study presents an analysis that explains the confinement of valence electrons in five Alkali atoms within the domains of a potential delineated by the function $\mathcal{V}(h,r,l,\alpha_c,a_l)$. The potential is devised to replicate the correct asymptotic behavior at large distances from the atomic core and is calibrated to align with the experimentally observed binding energy for the ground state at each angular momentum quantum number l. The method is well-suited for localized potentials and works well in finite domains having boundary conditions that are well known. The eigenvalue spectra provide a visualization of the energies of the Alkali species under the confining potential.

Keywords

Radial Probability Density, Wave Functions, Confining Potential

1. Introduction

The concept of confined atoms has attracted significant scholarly attention as a methodology for probing atomic and molecular behavior under spatial restrictions. These systems are particularly efficient for investigating how confinement influences fundamental atomic properties such as energy spectra and ionization thresholds [1]. Atomic confinement constitutes an indispensable theoretical framework across various disciplines. Within nuclear environments, confined atoms serve as analogs for examining nuclear matter under compression, with implications for phenomena such as nuclear compressibility, shell modifications in dense media, and nucleon localization in finite nuclear systems [2]-[5]. In liquid-state physics, it forms the basis of cell models, whereas in nanoscience, it facilitates the study of quantum dots and semiconductor nanostructures [1] [6]. Furthermore, the concept of confinement is pivotal for comprehending dense as-

trophysical conditions, such as ionized plasmas, white dwarf stars, and the interior structure of giant planets like Jupiter and Saturn [1] [2] [7]. Among the various paradigms investigated in numerous studies, the hydrogen atom confined within a cavity has been a subject of extensive research. Both spherical and ellipsoidal confinements have been analyzed using diverse quantum-mechanical methodologies. Research on hydrogen encapsulated within fullerene cages has also offered significant insights into endohedral complexes and nanoconfinement [2] [8]-[10]. Despite the structural resemblances between Alkali atoms and hydrogen, specifically due to the presence of a single valence electron, there have been relatively fewer detailed studies on confined Alkali species [2] [11]. Current research predominantly concentrates on computing total ground-state energies, for instance, for confined potassium (K) using Hartree—Fock configuration interaction methods and confined cesium (Cs) using Dirac—Fock calculations. However, comprehensive analyses of the effects of confinement on the excited-state spectra of Alkali atoms remain limited [2] [3] [7]. In this study, I employed a model potential approach, as outlined in [2], to characterize the valence electron of Alkali ions in specified excited states. This potential is devised to replicate the correct asymptotic behavior at large distances from the atomic core and is calibrated to align with the experimentally observed binding energy for the ground state at each angular momentum quantum number l [6] [12] [13]. It also affords precise forecasts for excited-state energies. To represent spatial confinement, I integrated this model potential with a spherical infinite-wall potential (impenetrable wall at finite radius R). This composite potential framework enables the calculation of the energy spectrum of the valence electron as a function of the confining radius R, thereby providing insights into how confinement influences the electronic structure of Alkali atoms.

2. Theory

A brief review of relevant mathematical concepts is necessary to maintain continuity of thought and to facilitate a clear understanding of the procedure employed in this discussion.

The Schrödinger equation that governs the energy eigenfunctions of confined Alkali species modeled by a Hamiltonian comprising a system of nucleons and a single valence electron is given by:

$$\hat{\mathcal{H}} = \frac{\hat{p}_1^2}{2m_1} + \frac{\hat{p}_2^2}{2m_2} - V\left(\hat{x}_2 - \hat{x}_1\right), \tag{1}$$

where ($\hat{p}_1, \hat{x}_1$) represent the momenta and coordinates for the nucleus and electron, m_1 indicates the mass of the nucleus, m_2 that of the electron, respectively [1] [7] [8]. This expression depicts a typical two-body problem, where mathematics teaches separating variables as a way of demystifying into center of mass and relative motion. To this end, one introduces the center of mass frame with $\hat{R} = \left(m_1\hat{x}_1 + m_2\hat{x}_2\right)/M$, with $M = m_1 + m_2$ and the total momentum $\hat{P} = \hat{p}_1 + \hat{p}_2$.

Concerning the relative motion, an obvious coordinate is the relative coordinate $\hat{x}=\hat{x}_2-\hat{x}_1$ and the relative momentum is $\hat{p}=\frac{m_1}{M}\hat{p}_2-\frac{m_2}{M}\hat{p}_1$ satisfying canonical conjugate relation [8]. Therefore, solving Equation (1) by the method separation of variables:

$$\hat{\mathcal{H}}=\frac{\hat{P}^2}{2M}+\frac{\hat{p}^2}{2\mu}-V\left(|\hat{x}|\right) \tag{2}$$

The total wave-function can be written as $\Psi(R,x)=\Phi(R)\psi(x)$. The center of mass solution is a free particle problem, with the wave function $\Phi(R)=\Omega e^{\pm ikR}$ and the energy $E_k=\hbar^2k^2/2M$ [14], where Ω is a constant, it will henceforth be neglected. Also, we can use $\mu=m_1m_2/M$ as the reduced mass. The relative particle wave function $\psi(x)$ obeys the 3D problem:

$$\left[\frac{\hat{p}^2}{2\mu}-V\left(|\hat{x}|\right)\right]\psi(x)=E\psi(x) \tag{3}$$

A rearrangement and the introduction of the angular momentum term gives the momentum operator,

$$\hat{p}^2=-\hbar^2\frac{\partial^2}{\partial r^2}-\frac{2\hbar^2}{r}\frac{\partial}{\partial r}+\frac{\hat{L}^2}{r^2}, \tag{4}$$

where $\hat{L}$ is the angular momentum operator, such that we can construct functions of θ and ϕ known as spherical harmonics, which are common eigenfunctions of the operators $\hat{L}^2$ and $\hat{L}_z$ satisfying

$$\hat{L}^2Y_{l,m}(\theta,\phi)=\hbar^2l(l+1)Y_{l,m}(\theta,\phi) \tag{5}$$

$$\hat{L}_zY_{l,m}(\theta,\phi)=\hbar mY_{l,m}(\theta,\phi) \tag{6}$$

with integers l and $m=-l,\cdots,+l$. The next section introduces the potential model for the Alkali atoms of interest.

3. Alkali Atoms Potential Model

When the valence electron in an Alkali atom is far away from the core, its dominant interaction is due to the Coulomb term and the induced dipole moment, let $e=1$ [2] [8].

$$V\left(|\hat{x}|\right)\to V(x)=-\frac{1}{r}-\frac{\alpha_c}{2r^4};\ \text{for } r\to\infty \tag{7}$$

Here, α_c is the dipole polarizability of the core. At small distances from the center of the core, the Exclusion Principle gives rise to an effective strong short-range repulsion. We incorporate this effect by taking a model potential for the interaction between the core and the valence electron in a state of angular momentum l;

$$V_\ell(x)=\begin{cases}-\frac{1}{r}-\frac{\alpha_c}{2\left(r^2+a_l^2\right)^2}, & \text{for } r>a_l\\ \infty, & \text{for } r\le a_l\end{cases} \tag{8}$$

Here a_l is an l-dependent parameter that may be regarded as an effective hard-core radius. Taking a_l to be l-dependent is reasonable because exchange effects depend on the angular momentum. This assumption is similar to the usual quantum-defect description of excited atomic states, where the quantum defect is taken to be l-dependent [2] [7] [8]. Employing the instrumentation of the Laplacian aids the separation of variables, the wavefunction $\psi(x)$ becomes

$$\psi_{k,l,m}(x) = \mathcal{R}_{k,l}(r) Y_{l,m}(\theta,\phi) \tag{9}$$

where k is the radial quantum number, which labels the many possible solutions of the equation for $\mathcal{R}_{k,l}$ as:

$$-\frac{\hbar^2}{2\mu}\left[\frac{\partial^2}{\partial r^2}+\frac{2}{r}\frac{\partial}{\partial r}\right]\mathcal{R}_{k,l}+\left[\frac{\hbar^2 l(l+1)}{2\mu r^2}-\frac{1}{r}-\frac{\alpha_c}{2\left(r^2+a_l^2\right)^2}\right]\mathcal{R}_{k,l}=E_{k,l}\mathcal{R}_{k,l} \tag{10}$$

The normalization condition is also quite different from a 1D normalization, since it reads:

$$\int_0^\infty \mathrm{d}r r^2 \left|\mathcal{R}_{k,l}\right|^2 \tag{11}$$

Due to the non-trivial Hermitian radial momentum, we can define the radial wavefunctions as $u_{k,l}(r) = r\mathcal{R}_{k,l}(r)$ with normalization

$$\int_0^\infty \mathrm{d}r \left|u_{k,l}\right|^2 = 1, \tag{12}$$

this immediately verifies that the non-standard derivative terms for $\mathcal{R}_{k,l}$ become completely standard when written in terms of the derivatives of $u_{k,l}$:

$$\left[\frac{\partial^2}{\partial r^2}+\frac{2}{r}\frac{\partial}{\partial r}\right]\mathcal{R}_{k,l}=\frac{1}{r}\frac{\partial^2 u_{k,l}}{\partial r^2}, \tag{13}$$

satisfiing the half-line condition $[0,\infty)$, hence Equation (10) becomes:

$$-\frac{\hbar^2}{2\mu}\frac{\partial^2 u_{k,l}}{\partial r^2}+\left[\frac{\hbar^2 l(l+1)}{2\mu r^2}-\frac{1}{r}-\frac{\alpha_c}{2\left(r^2+a_l^2\right)^2}\right]u_{k,l}=E_{k,l}u_{k,l} \tag{14}$$

Let's eliminate all the physical constants ($\hbar,\mu$) by switching to dimensionless variables. Let us define a length a such that the potential energy and kinetic energy of confinement are of the same order, where we have used $e=1$,

$$\begin{cases} a=\dfrac{\hbar^2}{\mu} \\ E_H=\dfrac{\mu}{\hbar^2}, \end{cases} \tag{15}$$

which defines the Bohr radius with the corresponding dimensionless energy. Henceforth, we measure length in the units of a, energies in units of E_H, and mass in units of μ; these define a system of units called atomic units, often abbreviated as "a.u." [14]-[16]. If $\rho = r/a$ is the dimensionless length and $\tilde{\mathcal{E}} = E_{k,l}/E_H$ is the dimensionless energy, we can redefine the wavefunction as $f_l(p) = \sqrt{a}u_{k,l}(r)$ satisfying the dimensionless equation:

$$-\frac{1}{2}\frac{\partial^2 f_l}{\partial \rho^2}+\left[\frac{l(l+1)}{2\rho^2}-\frac{1}{\rho}-\frac{\alpha_c}{2\left(\rho^2+a_l^2\right)^2}\right]f_l=\tilde{\mathcal{E}}f_l \tag{16}$$

This equation is equivalent to using $\mu=e=\hbar=1$ in a standard Schrödinger equation in 1D on the half-line $[0,\infty)$. We continue with the use of r instead ρ, and E instead $\tilde{\mathcal{E}}$ such that the resulting radial equation becomes:

$$-\frac{1}{2}\frac{\mathrm{d}^2 f_l}{\mathrm{d}r^2}+\left[\frac{l(l+1)}{2r^2}-\frac{1}{r}-\frac{\alpha_c}{2\left(r^2+a_l^2\right)^2}\right]f_l=Ef_l \tag{17}$$

Next, we develop the computational finite difference approach.

4. The Method of Finite Difference

There are many other numerical approaches like, spectral, finite volume, finite element, etc., that can be considered to solve Equation (17), but the chosen method is well-suited for localized potentials and works well in finite domains having boundary conditions that are well known or asymptotically approximated. Equation (17) takes the form of a linear second-order differential equation with stable boundary conditions. Method involving finite difference for solving boundary value problems replaces each of the derivatives in the differential equation with an appropriate difference quotient approximation of the problem. The particular difference quotient and step size h are chosen to maintain a specified order of truncation error. However, h cannot be chosen too small because of the general instability of the derivative approximations [14]. The numerical treatment of valence electron wave function in a confined sphere will be easily solved by transforming Equation (17) to an eigenvalue-like problem. The finite difference method for the linear second-order boundary value problem becomes,

$$\frac{\mathrm{d}^2 f_l}{\mathrm{d}r^2}=-\left[2E-\frac{l(l+1)}{r^2}+\frac{2}{r}+\frac{\alpha_c}{\left(r^2+a_l^2\right)^2}\right]f_l, \tag{18}$$

for

$$f_l(r)=\begin{cases}0;\ \text{at } r=a_l\\ 0;\ \text{at } r=R\end{cases} \tag{19}$$

which requires that the difference quotient approximations be used to estimate $\frac{\mathrm{d}^2 f_l}{\mathrm{d}r^2}$. First, we choose an integer $N>0$ and divide the interval $[a_l,R]$ into equal subintervals of $(N+1)$ whose endpoints are the mesh points $r_i=a_l+ih$, for $i=0,1,\cdots,N+1$ where $h=(R-a_l)/(N+1)$.

$$\frac{\mathrm{d}^2 f_l(r)}{\mathrm{d}r^2}=-2Ef_l(r)-\left[-\frac{l(l+1)}{r^2}+\frac{2}{r}+\frac{\alpha_c}{\left(r^2+a_l^2\right)^2}\right]f_l(r) \tag{20}$$

Here, $\lambda(E)=-2E$ and $\xi_l(r)=\left[\frac{2}{r}-\frac{l(l+1)}{r^2}+\frac{\alpha_c}{\left(r^2+a_l^2\right)^2}\right]$ such that:

$$\frac{\mathrm{d}^2 f_l(r)}{\mathrm{d}r^2} = \lambda(E) f_l(r) - \xi_l(r) f_l(r) \tag{21}$$

The Taylor expansion of a function $f(x)$ gives

$f(x_0) + (x - x_0)\left.\frac{\mathrm{d}f}{\mathrm{d}x}\right|_{x_0} + \frac{(x-x_0)}{2!}\left.\frac{\mathrm{d}^2 f}{\mathrm{d}x^2}\right|_{x_0} + \cdots$, taking the sum of the expansions of $f(r+h)$ and $f(r-h)$ gives:

$$\frac{\mathrm{d}^2 f_l(r)}{\mathrm{d}r^2} = \frac{f_l(r+h) - 2f_l(r) + f_l(r-h)}{h^2} + \mathcal{O}(h^3) \tag{22}$$

For convenience, I modify the notations such that, $f_l(r) = f_i$, $f_l(r-h) = f_{i-1}$, and $f_l(r+h) = f_{i+1}$, where $i = 1, 2, \cdots, N$. Neglecting the negligible third-order terms, Equation (21) becomes,

$$\frac{f_{i+1} - 2f_i + f_{i-1}}{h^2} = \left[\lambda(E) - \xi_l^i\right] f_i \tag{23}$$

then we can rearrange terms such that we have,

$$f_{i+1} + \delta_i f_i + f_{i-1} = h^2 \lambda f_i \tag{24}$$

where I have used $\delta_i = h^2 \xi_l^i - 2$. Equation (24) is easily transformed into a symmetric matrix by using the boundary conditions $f_l(a_l) = f_0 = 0$ and $f_l(R) = f_{N+1} = 0$,

$$[\mathcal{M}] = \begin{bmatrix} \delta_1 & 1 & 0 & \cdots & & \mathcal{O} \\ 1 & \delta_2 & 1 & \cdots & & \\ 0 & 1 & \delta_3 & \ddots & & \\ \vdots & \ddots & \ddots & \ddots & \ddots & \\ & & & \delta_{N-2} & 1 & 0 \\ \mathcal{O} & & & 1 & \delta_{N-1} & 1 \\ & & & 0 & 1 & \delta_N \end{bmatrix}$$

$$f = \begin{bmatrix} f_1 \\ f_2 \\ \vdots \\ f_{N-1} \\ f_N \end{bmatrix}$$

This can simply be written in a compact form as:

$$[\mathcal{M}] f = \lambda(E) h^2 f \tag{25}$$

Hence, restoring the expression for $\lambda(E)$ gives

$$[\mathcal{M}] f = -2Eh^2 f, \tag{26}$$

further transformation turns this to,

$$[\mathcal{M}_\kappa] f = Ef, \tag{27}$$

where $[\mathcal{M}_\kappa] = \frac{1}{-2h^2}[\mathcal{M}]$. The symmetric matrix $[\mathcal{M}_\kappa]$ ensures physical

correctness, yields orthogonal eigenvectors that simplify analysis and guarantee completeness, enables efficient algorithms that save time and memory, enhances numerical stability, and preserves the inherent physical symmetry of the original differential system [8].

5. Results

This investigation offers a comprehensive analysis explaining the confinement of valence electrons in Li, Na, K, Rb, and Cs within a potential defined by the function $\mathcal{V}(h,r,l,\alpha_c,a_l)$. Confinement is understood to denote how the potential restricts the spatial distribution and energy of the electrons, whereby a reduced radial distance r indicates a more severe confinement, and a higher angular momentum quantum number l introduces a centrifugal barrier. This research refines data originally presented in Ref. [2], utilizing similar input parameters while providing additional explanations and interpretations. The computational matrix size is on the order of several tens of thousands. Precise values for the core's dipole polarizabilities are determined from Rydberg state energies [2] [6] and rigorous calculations. The parameter a_l is determined by ensuring that the minimal potential energy for a specified l corresponds with the experimentally observed lowest energy for the valence electron. Input values for the core's dipole polarizability, the minimal energy of the valence electron for a specified l, and the deduced values of the core radius a_l are presented in **Table 1**. The subsequent subsections elucidate the findings illustrated in **Tables 2-6**. The results conform with the Aufbau Principle of electronic configuration [17] as evidenced in the tables, which favors excitation into lower energy orbitals first.

Table 1. The input values of the core dipolar polarizabilities α_c, the lowest energy E_0 of the valence electron for a given $l=0$, and the implied values in atomic units (a.u.) of the core radius a_l [2] [8].

	Li	Na	K	Rb	Cs
α_c	0.192	0.99	5.5	9.2	15.7
$E_0(\text{eV})$	−5.392	−5.141	−4.340	−4.179	−3.894
a_0	0.833	0.963	1.436	1.595	1.857

Table 2. Energies $E(\text{eV})$ for various states of the valence electron in confined Li, for various confinement radii $R(\text{a.u.})$.

	$R\to\infty$	$R=20$	$R=15$	$R=10$	$R=7$	$R=5$	$R=4$	$R=3$
s	−5.392	−5.392	−5.392	−5.356	−4.918	−2.835	1.017	13.413
s	−2.009	−1.978	−1.746	0.003	5.531	19.827	40.506	98.482
s	−1.046	−0.345	1.252	7.628	22.846	58.180	107.161	241.229
s	−0.641	1.981	5.714	18.613	47.380	112.158	200.746	441.302
s	−0.431	5.125	11.597	32.869	79.048	181.673	321.171	698.615

Continued

p	−3.161	−3.160	−3.150	−2.920	−1.795	1.670	6.974	22.077
p	−1.428	−1.283	−0.731	1.980	8.890	25.111	47.525	108.426
p	−0.813	0.419	2.513	9.961	26.628	63.946	114.671	251.622
p	−0.525	2.906	7.162	21.171	51.418	118.183	208.497	451.891
d	−1.512	−1.469	−1.269	−0.190	2.653	9.132	17.544	38.418
d	−0.850	−0.150	1.110	5.547	15.110	35.315	61.363	128.303
d	−0.544	1.862	4.836	14.349	34.019	75.487	129.790	272.543

Table 3. Energies $E(\text{eV})$ for various states of the valence electron in confined Na, for various confinement radii $R(\text{a.u.})$.

	$R\to\infty$	$R=20$	$R=15$	$R=10$	$R=7$	$R=5$	$R=4$	$R=3$
s	−5.141	−5.141	−5.141	−5.093	−4.565	−2.144	2.354	17.286
s	−1.944	−1.906	−1.640	0.281	6.284	22.018	45.360	113.693
s	−1.021	−0.258	1.433	8.160	24.385	62.920	117.890	275.299
s	−0.628	2.116	5.995	19.480	50.005	120.453	219.684	501.750
s	−0.424	5.313	11.999	34.161	83.065	194.530	350.652	792.969
p	−3.134	−3.133	−3.122	−2.880	−1.698	1.999	7.812	25.163
p	−1.416	−1.264	−0.693	2.111	9.348	26.779	51.631	122.493
p	−0.807	0.455	2.598	10.282	27.781	68.038	124.512	284.401
p	−0.522	2.969	7.317	21.782	53.595	125.757	226.472	510.980
d	−1.516	−1.473	−1.276	−0.205	2.628	9.156	17.819	40.326
d	−0.852	−0.155	1.100	5.537	15.203	36.145	64.126	140.133
d	−0.545	1.854	4.828	14.402	34.540	78.346	137.859	302.696

Table 4. Energies $E(\text{eV})$ for various states of the valence electron in confined K, for various confinement radii $R(\text{a.u.})$.

	$R\to\infty$	$R=20$	$R=15$	$R=10$	$R=7$	$R=5$	$R=4$	$R=3$
s	−4.341	−4.341	−4.339	−4.217	−3.236	0.917	9.012	40.738
s	−1.732	−1.655	−1.238	1.404	9.489	32.176	69.832	205.079
s	−0.936	0.080	2.138	10.309	30.956	84.856	171.823	479.479
s	−0.586	2.635	7.091	22.991	61.210	158.780	314.749	863.725
s	−0.398	6.035	13.563	39.389	100.188	253.885	498.555	1357.780
p	−2.963	−2.962	−2.944	−2.619	−1.077	4.070	13.141	46.585
p	−1.340	−1.155	−0.475	2.834	11.793	35.645	74.319	211.240
p	−0.777	0.653	3.046	11.895	33.416	88.470	176.432	485.722
p	−0.505	3.297	8.089	24.668	63.754	162.460	319.409	869.998
d	−1.529	−1.489	−1.296	−0.233	2.688	10.034	21.184	58.193
d	−0.856	−0.167	1.095	5.688	16.393	42.605	83.318	223.580
d	−0.547	1.858	4.900	15.108	38.390	95.745	185.684	498.222

Table 5. Energies $E(\text{eV})$ for various states of the valence electron in confined Rb, for various confinement radii $R(\text{a.u.})$.

	$R\to\infty$	$R=20$	$R=15$	$R=10$	$R=7$	$R=5$	$R=4$	$R=3$
s	−4.179	−4.179	−4.176	−4.026	−2.878	1.995	11.841	53.862
s	−1.683	−1.593	−1.127	1.750	10.612	36.313	81.083	257.660
s	−0.916	0.176	2.349	11.020	33.393	94.067	197.050	597.722
s	−0.576	2.787	7.432	24.202	65.471	175.075	359.515	1073.872
s	−0.392	6.255	14.068	41.237	106.786	279.280	568.438	1686.083
p	−2.929	−2.928	−2.908	−2.557	−0.878	4.917	15.656	59.232
p	−1.333	−1.125	−0.410	3.081	12.735	39.487	85.171	263.247
p	−0.769	0.714	3.193	12.482	35.641	97.351	201.224	603.367
p	−0.501	3.403	8.354	25.737	67.785	178.409	363.727	1079.532
d	−1.540	−1.501	−1.313	−0.257	2.713	10.528	23.153	69.929
d	−0.860	−0.177	1.087	5.763	16.996	45.860	93.367	274.432
d	−0.548	1.857	4.934	15.451	40.186	103.954	209.598	614.649

Table 6. Energies $E(\text{eV})$ for various states of the valence electron in confined Cs, for various confinement radii $R(\text{a.u.})$.

	$R\to\infty$	$R=20$	$R=15$	$R=10$	$R=7$	$R=5$	$R=4$	$R=3$
s	−3.895	−3.895	−3.890	−3.675	−2.178	4.244	18.134	88.981
s	−1.601	−1.482	−0.923	2.398	12.760	44.668	105.552	397.173
s	−0.881	0.350	2.731	12.324	37.980	112.521	251.674	911.061
s	−0.559	3.061	8.044	26.397	73.442	207.628	456.323	1630.540
s	−0.380	6.644	14.963	44.564	119.092	329.946	719.468	2555.593
p	−2.837	−2.836	−2.810	−2.393	−0.404	6.842	21.516	93.704
p	−1.297	−1.058	−0.268	3.593	14.640	47.451	109.114	402.011
p	−0.752	0.841	3.490	13.617	39.949	115.375	255.288	915.924
p	−0.491	3.614	8.864	27.744	75.456	210.513	459.958	1635.412
d	−1.551	−1.513	−1.327	−0.257	2.896	11.919	28.223	103.137
d	−0.862	−0.177	1.111	6.014	18.421	53.034	116.250	411.689
d	−0.549	1.886	5.060	16.245	43.921	121.101	262.526	925.652

1) Alkali Spectra

The eigenvalue spectra provide a visualization of the energies of the Alkali systems under the confining potential. **Figure 1** displays the first five energy levels $(E_1, E_2, E_3, E_4, E_5)$ in (eV) as a function of the quantum number n (ranging from 1 to 5) for each quantum number of angular momentum $l=0,1,2$ and the radial extent r $(\infty, 20, 15, 10, 7, 5, 4, 3)$ in (a.u.). This section explains the spectra significance in the context of the radial expression in Equation (17). The spacing

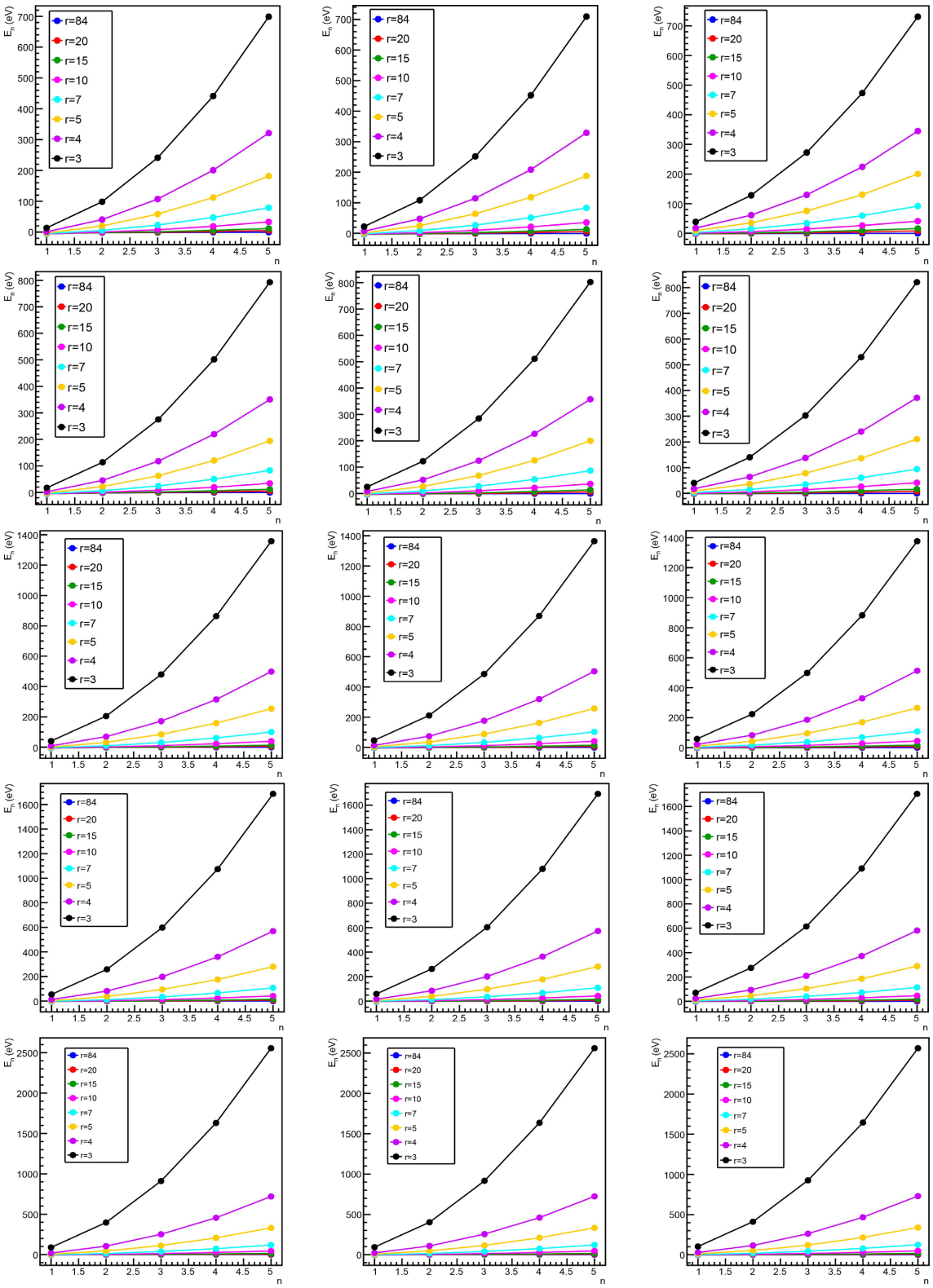

Figure 1. Illustration of the energy spectra for each angular momentum value $l=0,1,2$, these plots show the first five eigenvalues (E_1,E_2,E_3,E_4,E_5) in eV against their index $n=1,2,3,4,5$ with separate curves for each r. Each curve represents the energy spectrum at a fixed r,l. Each plot's row represents the Alkali species, *i.e.,* Li, Na, K, Rb, and Cs; and each column gives $l=0,1,2$ dependence, respectively. Angular momentum values $l=1,2$ include further extrapolation of eigen energies.

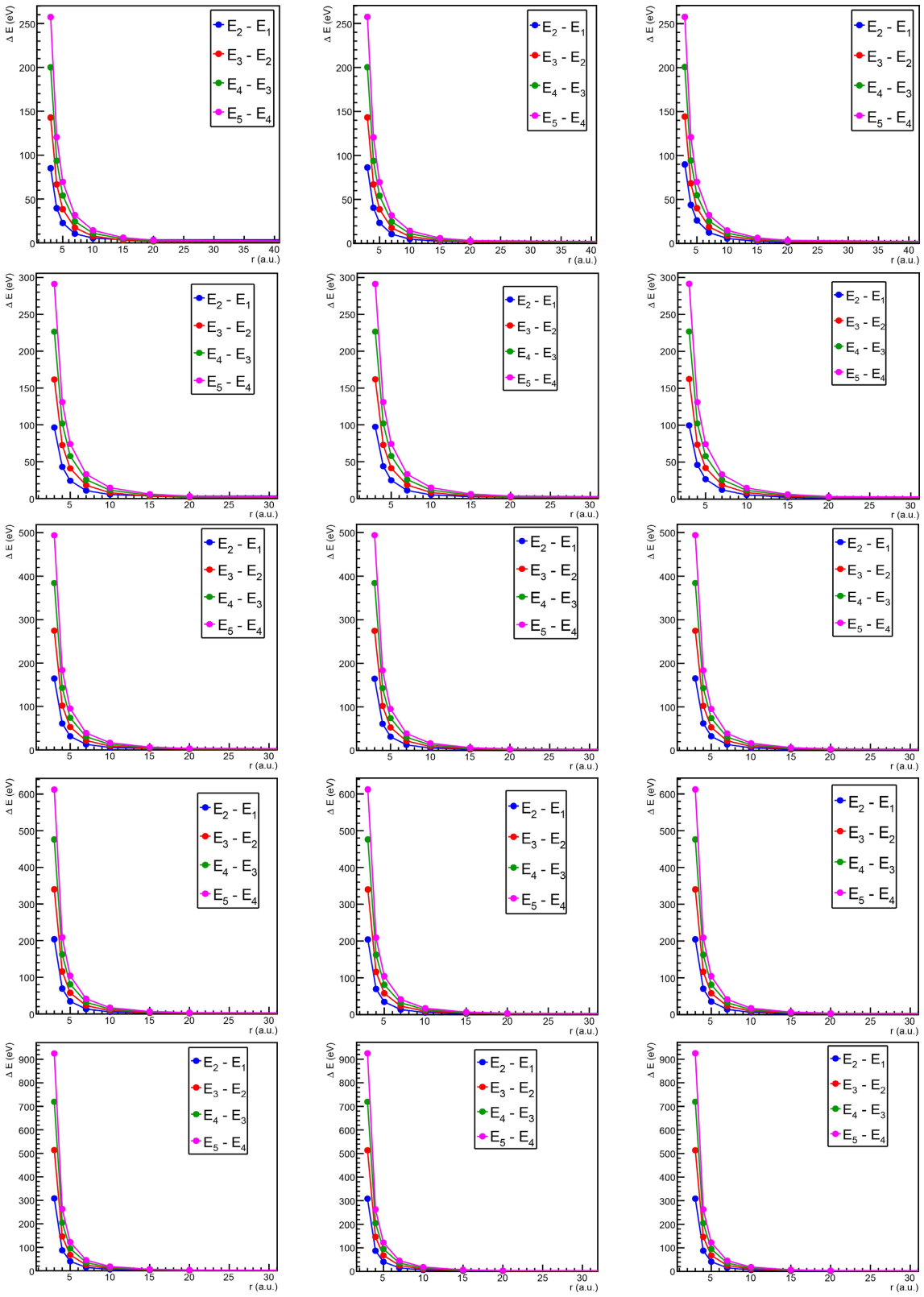

Figure 2. The energy difference plot of Alkali species, such that for each $l = 0,1,2$, these plots depict $\Delta E_n = E_{n+1} - E_n$ in eV against r, with separate curves for each $n = 1,2,3,4$. Each plot's row represents the Alkali species, *i.e.*, Li, Na, K, Rb, and Cs; and each column gives $l = 0,1,2$ dependence, respectively. Angular momentum values $l = 1,2$ include further extrapolation of eigen energies.

between energy levels $\left(E_{n+1}-E_n\right)$ indicates the degree of confinement. Smaller r results in larger energy level spacings, as the electron is confined to a smaller region, increasing quantization. Larger r allows the wavefunction to spread, reducing spacings and approaching a continuum-like spectrum. In terms of the angular momentum, the higher l increases the centrifugal barrier ($l\left(l+1\right)/r^2$), raising all energy levels and potentially altering the confinement. For $l=0$, the absence of the centrifugal term leads to lower energies indicating less confinement resistance. The plots show how the energy spectra become more discrete at smaller r, reflecting stronger confinement. For example, at $r=3$, the levels are widely spaced, while at $r\to\infty$, they are closer, resembling a less confined system.

2) Energy Difference Predicting Confinement

The energy differences are computed based on the energies obtained from solving Equation (17). The larger ΔE_n at smaller r means stronger confinement, as the potential compresses the wavefunction, increasing energy level distances. As r becomes bigger, ΔE_n becomes smaller, indicating a less confined system where levels are closer together. **Figure 2** gives these energy differences. The higher l indicates a centrifugal barrier, which may reduce ΔE_n for some n, as the effective potential becomes shallower at larger r. For $l=0$, the Coulomb term dominates, this leads to a larger ΔE_n at small r.

3) Alkali Radial Probability Density and Wave Functions

The radial probability density facilitates a comprehensive understanding of the spatial distribution of an electron's probability within a potential's confines. These plots display $\left|x\psi_1\left(x\right)\right|^2$, the radial probability density. The computation of the radial probability density utilizes the ground state wavefunction $\psi_1\left(x\right)$, corresponding to the first eigenfunction obtained from the solution of Equation (17). The plots in **Figure 3** quantitatively assess the strength of confinement. For example, a pronounced increase in ΔE_1 as r decreases from ∞ to 3 indicates a transition to a state characterized by pronounced confinement. Variations across n demonstrate the distinct effects of confinement on excited states. The radial probability density $\left|x\psi_1\left(x\right)\right|^2$ encapsulates the spherical symmetry of the system by incorporating the squared wavefunction together with the surface area element $4\pi x^2$. This conjunction is integrated across angles within a three-dimensional framework, approximated in this context by x^2 for the radial component. This dimension serves as a more physically significant metric than the wavefunction itself, reflecting the likelihood per unit radial distance of finding the electron. In the case of $l=0$, the peak of $\left|x\psi_1\left(x\right)\right|^2$ in close proximity to $x=r_1$ denotes the most probable radius, predominantly dictated by Coulomb attraction. Conversely, for $l>0$, the centrifugal barrier induces an outward displacement of this peak. The higher l shifts the peak of $\left|x\psi_1\left(x\right)\right|^2$ to larger x, due to the centrifugal barrier pushing the electron away from the origin. For $l=0$, the peak is closest to $x=r_1$. The plots show where the electrons are most likely located. A sharp peak at small r indicates strong localization, while a broad distribution at large r suggests a delocalized electron - the shift for higher l highlights angular

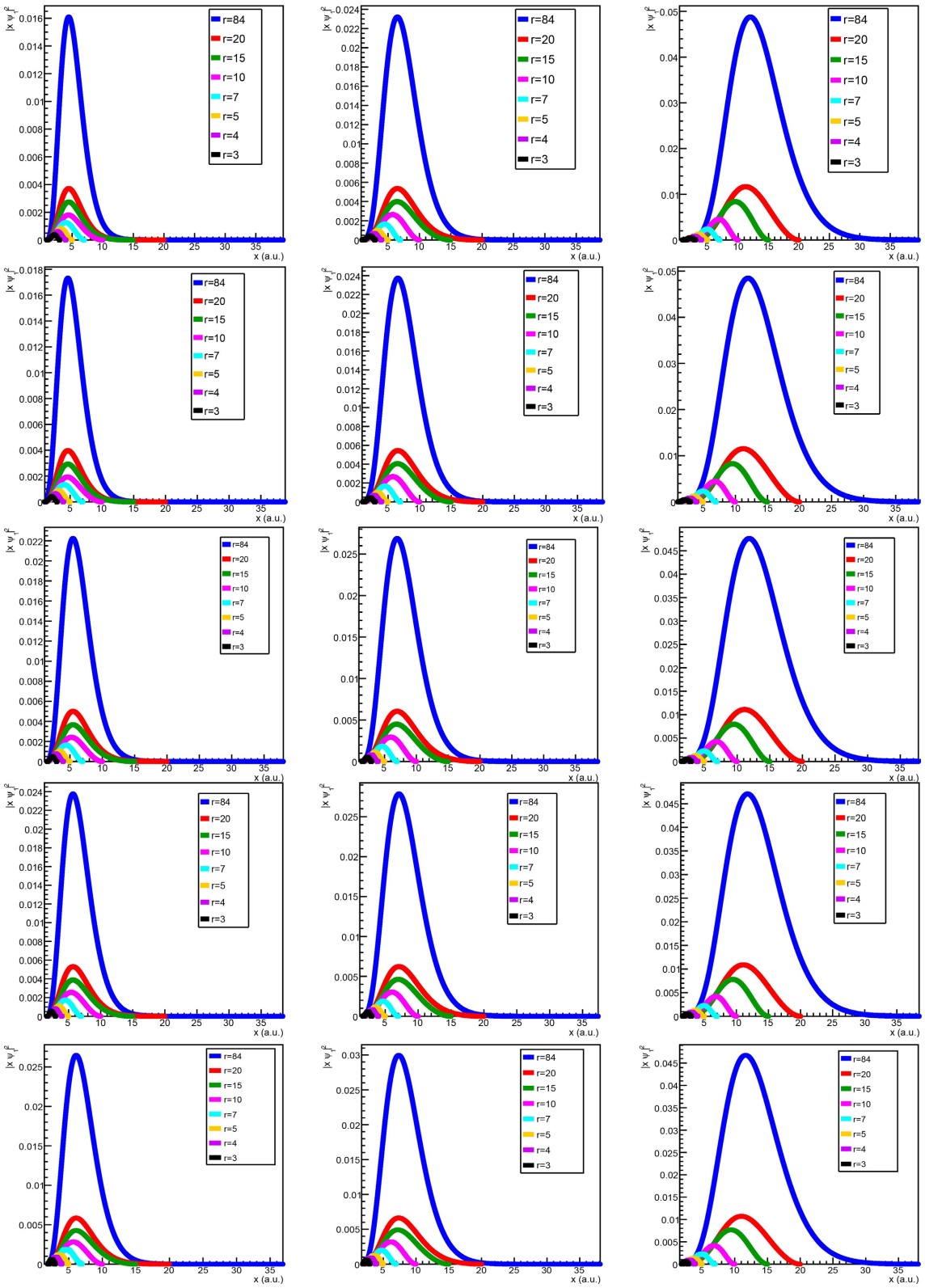

Figure 3. The radial probability density $\left|x\psi\left(x\right)\right|^2$ for each of the angular momentum proportional to the probability of finding the electron at radius x, with curves for each r. Each plot's row represents the Alkali species, *i.e.*, Li, Na, K, Rb, and Cs; and each column gives $l=0,1,2$ dependence, respectively. Angular momentum values $l=1,2$ include further extrapolation of eigen energies.

momentum's role in reducing confinement near the core. Figure 4 shows the 2D illustration of the wavefunctions resulting from the solution to Equation (17).

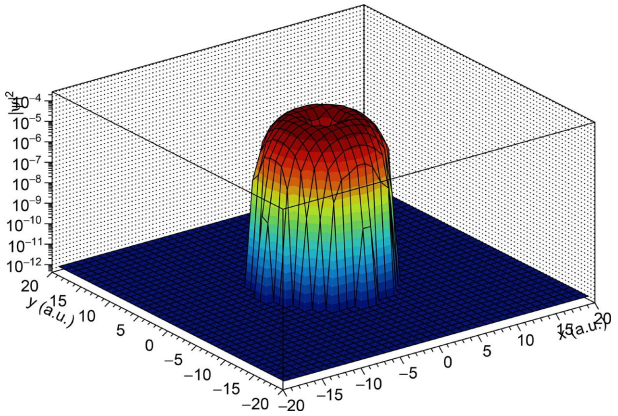

Figure 4. Spatial visualization of the probability density $|\psi(x,y)|^2$ for the ground state wavefunction of Li for $r=10$.

4) Effective Potential of Alkali Species

The form of the potential function signifies confinement. The Coulomb term $(-2/x^2)$ serves to attract the electron towards the nucleus, while the core term $(\alpha_c/(x^2+a_l^2)^2)$ introduces a short-range repulsion. In contrast, the centrifugal term $(l(l+1)/x^2)$ effectuates repulsion when $l>0$. A reduction in r truncates the potential at a lesser value of R, thus elevating the energy levels by diminishing the electron's available space.

As illustrated in Figure 5, when considering $l=0$, the potential is devoid of the centrifugal term, thereby forming a profound well predominantly influenced by Coulomb attraction, resulting in substantial confinement. Conversely, for $l=1,2$, the centrifugal barrier increases the potential near the nucleus, thereby diminishing confinement by displacing the electron outward.

The graphical representations elucidate why energy levels increase (become less negative) for lower values of r: the truncated potential well becomes both shallower and narrower. The centrifugal barrier at higher l values demonstrates why E_1 is elevated, as the electron experiences less confinement near the nucleus.

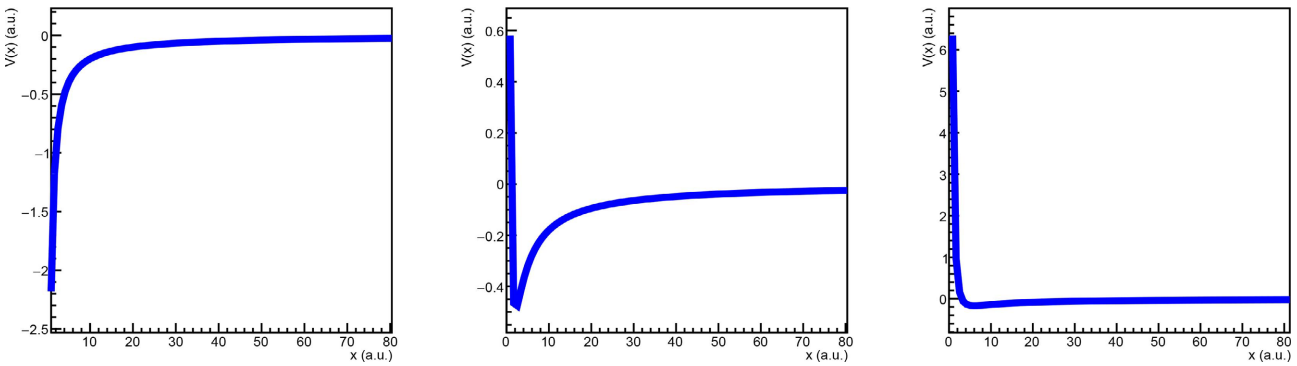

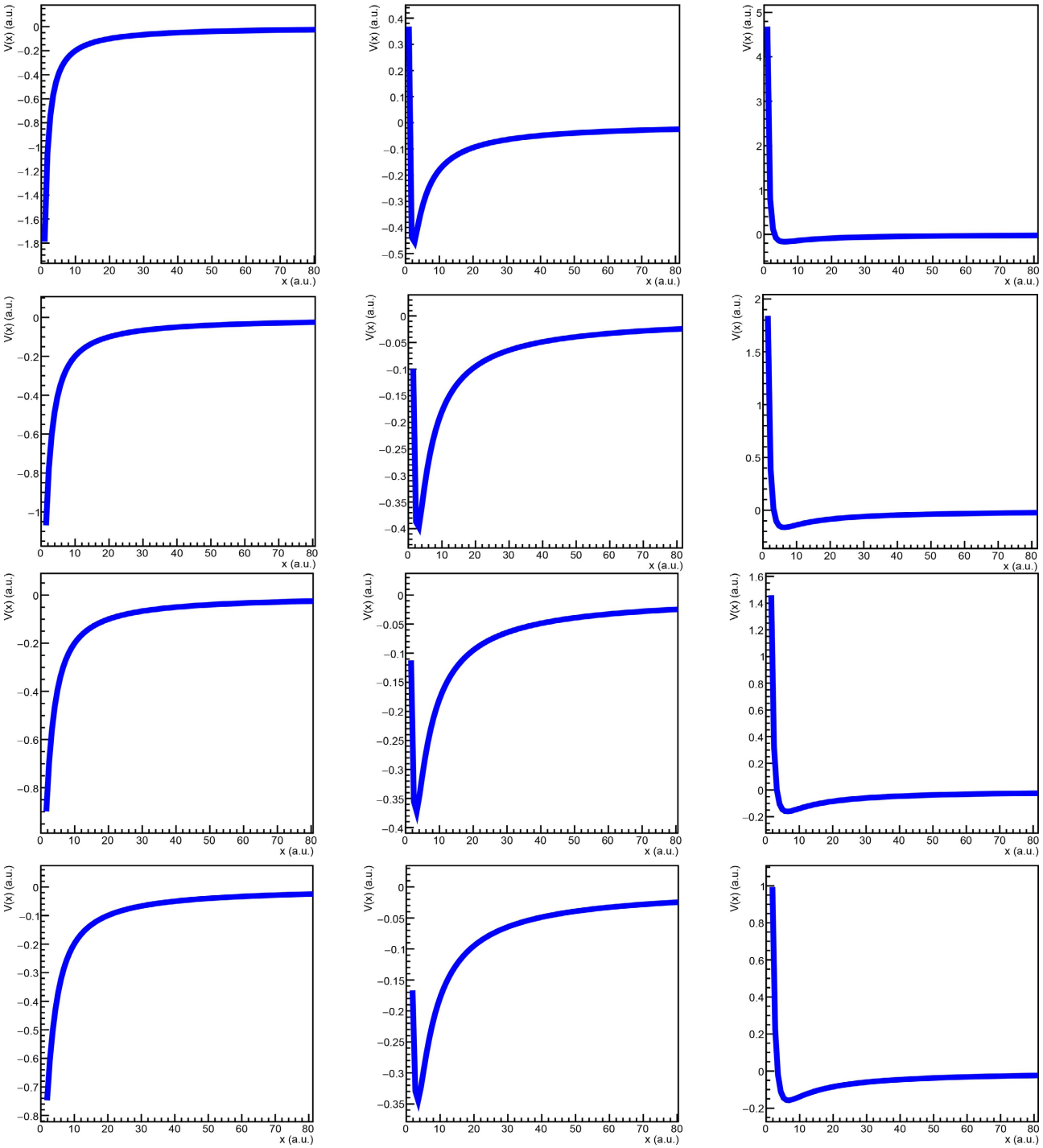

Figure 5. For each $l=0,1,2$, these plots show the effective potential $V(x)=\frac{l(l+1)}{x^2}-\frac{2}{x}+\frac{\alpha_c}{\left(x^2+a_l^2\right)^2}$ in atomic units against x. Each plot's row represents the Alkali species, *i.e.*, Li, Na, K, Rb, and Cs; and each column gives $l=0,1,2$ dependence respectively.

6. Conclusion

This study offers an in-depth analysis of the quantum confinement phenomena

observed in Alkali elements within a custom l dependent potential. The eigenvalue spectrum plots exhibit discrete energy levels that ascend with an increase in the quantum number, attributing higher energies and increased spacing to smaller radial extents owing to enhanced confinement; conversely, larger radial extents correspond to reduced energies and diminished spacing. The centrifugal component raises energy levels compared to $l=0$, indicative of its repulsive nature. Analysis of energy difference plots corroborates that ΔE_n increases as r decreases, with $l=0$ demonstrating maximal spacing at minimal r, which is tempered by the centrifugal barrier at elevated l. The core potential (α_c, α_l) governs these variations, inferring the presence of a wider, albeit slightly weaker, potential well that significantly influences the electronic configuration. The radial probability density plots display a concentrated distribution proximal to $x=r_1$ for $l=0$, shifting outward for $l=1,2$, with more acute peaks arising from heightened confinement at reduced r, whereas the 2D wavefunction density plot showcases a centrally symmetric peak for $l=0$ and r that attenuates towards the periphery, moderated by the core's repulsive force. The high grid resolution employed in n guarantees accuracy, meticulously capturing the detailed variations across the parameters.

Acknowledgements

I express my deepest gratitude to the East African Institute for Fundamental Research (ICTP-EAIFR) for providing exceptional training that has significantly enhanced my research capabilities. Their commitment to fostering scientific excellence in the region is truly commendable. I am also sincerely thankful to Prof. Steven Ndengue for his generous advice and invaluable guidance, which have been instrumental in shaping this work. This study received no external funding from any organization or agency.

Conflicts of Interest

The author declares no conflicts of interest regarding the publication of this paper.

References

[1] Dolmatov, V.K., Baltenkov, A.S., Connerade, J. and Manson, S.T. (2004) Structure and Photoionization of Confined Atoms. *Radiation Physics and Chemistry*, **70**, 417-433. https://doi.org/10.1016/j.radphyschem.2003.12.024

[2] Patil, S.H., Sen, K.D. and Varshni, Y.P. (2005) Alkali Atoms Confined to a Sphere and to a Fullerene Cage. *Canadian Journal of Physics*, **83**, 919-928. https://doi.org/10.1139/p05-023

[3] Patil, S.H. and Varshni, Y.P. (2009) Properties of Confined Hydrogen and Helium Atoms. In: *Advances in Quantum Chemistry*, Elsevier, 1-24. https://doi.org/10.1016/s0065-3276(09)00605-4

[4] Hillier, I.H. and Walkley, J. (1964) Quantum Cell Model. I. the Uniform Potential Approximation. *The Journal of Chemical Physics*, **41**, 3205-3212. https://doi.org/10.1063/1.1725698

[5] Fletcher, L.N., Kaspi, Y., Guillot, T. and Showman, A.P. (2020) How Well Do We Understand the Belt/Zone Circulation of Giant Planet Atmospheres? *Space Science Reviews*, **216**, Article No. 30. https://doi.org/10.1007/s11214-019-0631-9

[6] Melono, R.L.M., Etindélé, A.J., Tchakoua, T., Ndengué, S.A. and Motapon, O. (2015) Polarizability of Off-Center Spherically Confined Hydrogen Atom. *Journal of Physics B*: *Atomic*, *Molecular and Optical Physics*, **48**, Article 215001. https://doi.org/10.1088/0953-4075/48/21/215001

[7] Melono, R.L.M., Doba, P., Etindele, A.J. and Motapon, O. (2020) Oscillator Strengths, Transition Probabilities and State Lifetimes of Hydrogen Atom Confined in Spherical Cavity: Off-Center Displacement Effects. *Physica Scripta*, **95**, Article 055401. https://doi.org/10.1088/1402-4896/ab7144

[8] Patil, S.H. and Varshni, Y.P. (2006) Hydrogenic System Confined to a Two-Dimensional Circular Disc. *Canadian Journal of Physics*, **84**, 165-180. https://doi.org/10.1139/p06-049

[9] Changa, M.E., Scherbinin, A.V. and Pupyshev, V.I. (2000) Perturbation Theory for the Hydrogen Atom in a Spherical Cavity with Off-Centre Nucleus. *Journal of Physics B*: *Atomic*, *Molecular and Optical Physics*, **33**, 421-432. https://doi.org/10.1088/0953-4075/33/3/311

[10] Changa, M.E., Scherbinin, A.V. and Pupyshev, V.I. (2003) Spectra of One-Electron Atom in a Spherical Cavity. *International Journal of Quantum Chemistry*, **96**, 167-174. https://doi.org/10.1002/qua.10637

[11] Martínez-Flores, C. and Cabrera-Trujillo, R. (2020) High Pressure Effects on the Excitation Spectra and Dipole Properties of Li, Be^{+}, and B^{2+} Atoms under Confinement. *Matter and Radiation at Extremes*, **5**, Article 024401. https://doi.org/10.1063/1.5139099

[12] Guillot, T. (1999) A Comparison of the Interiors of Jupiter and Saturn. *Planetary and Space Science*, **47**, 1183-1200. https://doi.org/10.1016/s0032-0633(99)00043-4

[13] Hastenrath, S. and Greischar, L. (1993) Changing Predictability of Indian Monsoon Rainfall Anomalies? *Journal of Earth System Science*, **102**, 35-47. https://doi.org/10.1007/bf02839181

[14] Hadi, M. (2011) Lectures on Quantum Mechanics.

[15] Amusia, M.Y., Baltenkov, A.S., Dolmatov, V.K., Manson, S.T. and Msezane, A.Z. (2004) Confinement Resonances in Photoelectron Angular Distributions from Endohedral Atoms. *Physical Review A*, **70**, Article 023201. https://doi.org/10.1103/physreva.70.023201

[16] Baltenkov, A.S., Dolmatov, V.K., Manson, S.T. and Msezane, A.Z. (2004) Nondipole Effects in the Photoabsorption of Electrons in Two-Centre Zero-Range Potentials. *Journal of Physics B*: *Atomic*, *Molecular and Optical Physics*, **37**, 3837-3846. https://doi.org/10.1088/0953-4075/37/19/005

[17] Park, B.S. and Stetten, D. (2001) A Principle Written in Diagrams: The Aufbau Principle for Molecules and Its Visual Representations, 1927-1932. In: *Boston Studies in the Philosophy and History of Science*, Springer, 179-198. https://doi.org/10.1007/978-94-015-9737-1_11